Research Article Vol. 14, No. 5 / 1 May 2023 / Biomedical Optics Express 2117
Biomedical Optics EXPRESS

Blind deconvolution of second harmonic microscopy images of the living human eye

ROSA M. MARTÍNEZ-OJEDA,[1] LAURENT M. MUGNIER,[2] PABLO ARTAL,[1] AND JUAN M. BUENO[1,*]

[1]Laboratorio de Óptica, Instituto Universitario de Investigación en Óptica y Nanofísica, Universidad de Murcia, Campus de Espinardo (Ed. 34), 30100 Murcia, Spain
[2]ONERA / DOTA, Université Paris Saclay, F-92322 Châtillon, France
*bueno@um.es

Abstract: Second harmonic generation (SHG) imaging microscopy of thick biological tissues is affected by the presence of aberrations and scattering within the sample. Moreover, additional problems, such as uncontrolled movements, appear when imaging *in-vivo*. Deconvolution methods can be used to overcome these limitations under some conditions. In particular, we present here a technique based on a marginal blind deconvolution approach for improving SHG images obtained *in vivo* in the human eye (cornea and sclera). Different image quality metrics are used to quantify the attained improvement. Collagen fibers in both cornea and sclera are better visualized and their spatial distributions accurately assessed. This might be a useful tool to better discriminate between healthy and pathological tissues, especially those where changes in collagen distribution occur.

© 2023 Optica Publishing Group under the terms of the Optica Open Access Publishing Agreement

1. Introduction

Second harmonic generation (SHG) imaging is a form of nonlinear, or multiphoton (MP), microscopy being used in different areas of biomedical research. It has been shown to be especially useful in the visualization of variety of collagen-based tissues [1–3]. This technique provides intrinsic confocality, reduced photodamage and does not require the use of external markers.

A particular application of SHG microscopy has been the characterization of the ocular structures with a high collagen content. Although Hochheimer demonstrated SHG signal from the corneal tissue in 1982 [4], it wasn't until 2002 when the first SHG images of the corneal stroma (from a rabbit) were reported by Yeh et al. [5]. Since then, several authors have shown this imaging procedure as an efficient and accurate tool to investigate the three-dimensional collagen structure of the human cornea at high spatial resolution [6–8]. Moreover, the changes in corneal collagen distribution produced by pathologies and surgery have also been explored by means of SHG microscopy [9,10]. Unlike the cornea, studies reporting SHG images on the human sclera are not as numerous [11–14].

Although there has been an increasing interest in SHG microscopy in human ocular tissues, most studies were centred exclusively on samples from donors (i.e. in *ex vivo* experimental conditions). Some experiments used *in vivo* animal models, but their success was limited, and tissue labelling was often applied to increase the detected nonlinear signal [15–19]. To the best of our knowledge, up to now, our group has been the only one to successfully report SHG images of the living human eye in both the cornea and the sclera [20].

Despite SHG optical sectioning capabilities, the quality of the images (both contrast and resolution) is mainly limited by sample-induced aberrations [21]. This indicates that SHG images worsen as depth within the tissue increases. This effect also occurs when imaging tissues with a high degree of transparency such as the cornea [22,23]. To overcome this limitation, adaptive optics (AO) technology has been implemented into MP imaging microscopes. For more than

#486989 https://doi.org/10.1364/BOE.486989
Journal © 2023 Received 3 Feb 2023; revised 17 Mar 2023; accepted 19 Mar 2023; published 19 Apr 2023

Biomedical Optics EXPRESS

20 years, different MP-AO approaches have been proposed to deal with this natural limitation (see [24–26] as general references). Although these procedures are broadly used to correct for aberrations in static samples, their implementation when imaging thick dynamic/living specimens has also reported interesting and useful results in different living tissues including mouse embryos [27], and mouse, zebrafish and fly brains [28–30].

These techniques are also useful for MP imaging of *in vivo* thick ocular tissues. The living human eye is a paradigmatic example where involuntary micro-movements exist. In addition, the short exposure time to allow safe recording conditions might also add noise due to a low light level conditions. Then, apart from the limitations due to specimen-induced aberrations, MP imaging of the *in vivo* human eye are affected by these factors and produce images with a lower quality. Since AO devices often become complex and costly when living specimens are involved, alternative methods such deconvolution might be also useful for image improvement.

Deconvolution techniques have long been popular methods to improve the quality of microscopy images, with or without AO. Numerous approaches have been applied to the different types of microscopy, including wide-field fluorescence, confocal and structured illumination, and more recently also for MP imaging [31–37]. Deconvolution is a class of post-processing methods able to deblur images, which usually requires information about the point spread function (PSF). Deconvolution of SHG images of the human cornea and the sclera is difficult because the PSF is not well-known. Then, we must therefore estimate both the PSF and the object, what is known as blind or myopic deconvolution [38].

In this work we propose an approach based on the so-called *marginal blind deconvolution*. This image restoration method is based on a sound statistical framework that avoids the usual degeneracies encountered in blind deconvolution and makes it entirely unsupervised [39]. We used the method to improve the quality of SHG images of different ocular structures of the living human eye acquired with a compact MP microscope.

2. Methods

2.1. Compact multiphoton microscope

The experimental setup is a custom, compact and clinically-adapted prototype MP microscope (Fig. 1) [20]. In brief, the device uses a Ti:sapphire femtosecond laser (800 nm, 76 MHz) as illumination source. The collimated beam passes a XY scanning (dual-axis galvo unit), a telescopic system composed of two achromatic doublets (L1 and L2) and a dichroic mirror (DIC) before reaching the eye through a non-immersion microscope objective (OB, 20×, NA = 0.50). OB allows non-contact operation during imaging acquisition due to its long working-distance (20 mm). SHG signal coming from the ocular structures are collected via the same objective, and DIC separates it from the infrared light used for excitation. These signals pass a spectral filter and reach the detection unit (PMT). SHG signals from the cornea and the sclera are isolated by means of a narrow-band spectral filter (400 ± 10 nm). A motorized actuator coupled to OB corrects for the focus position along the Z direction. A continuously variable neutral density filter (NDF) and an electro-mechanical shutter (S) placed in front of the scanning unit laser allow safe light levels and appropriate exposures times. A XYZ chinrest and two additional CCD cameras help to control for the correct position of the eye/sample under study. A fixation target facilitates stability and minimizes ocular movements during measurements.

SHG images (0.42-s exposure time) from different ocular structures and locations were acquired in healthy volunteers. Only individual frames were used here (i.e. “raw” images, no averaged ones) and these entered the deconvolution algorithm described in the next section. The entire imaging protocol was controlled and synchronized through custom C++ software. Further details on this instrument can be found in [20].

The quality of the images was assessed with objective metrics such as intensity profiles, acutance [40], and sparsity and dominant orientation-based quality image estimation (SDQI) [41].

Biomedical Optics EXPRESS

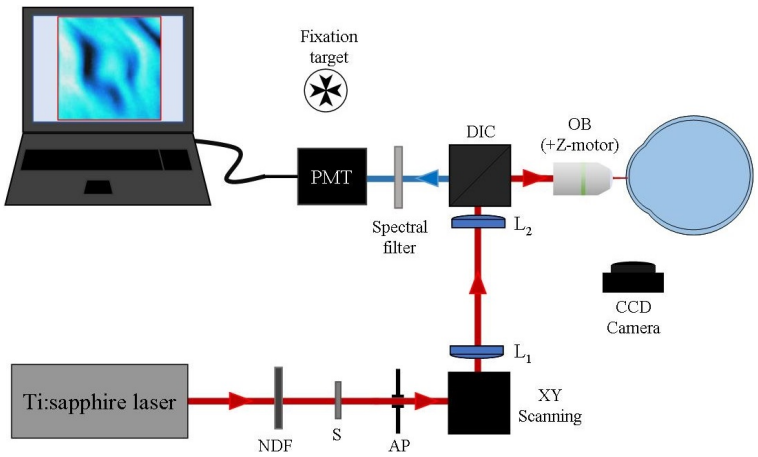

Fig. 1. Schematic diagram of the compact MP microscope. NDF, neutral density filter; S, shutter; AP, aperture; DIC, dichroic mirror. PMT, photomultiplier tube. The experimental system is mounted on a 30×30 cm^2 platform (laser excluded).

SDQI is a prominent no-reference image quality assessment method developed by the image processing community. This metric allows an accurate evaluation of the quality of the SHG image considering the gradient of the structures and the local dominant orientation within the images, measuring the effective image signal and the possible noise content of each local region in the Fourier domain. Higher values of SDQI correspond to images with more recognizable feature content, greater contrast and better resolution (i.e. increased local gradient), all factors associated to a superior image quality [42,43]. In a similar way to acutance, SDQI metric can also be used to classify collagen organization [43,44]. In that sense larger (smaller) values of SDQI indicate high (low) level of organization of the collagen fibers within the analyzed sample. This part of the image processing, as well as the one below described were performed with MatLab.

In addition, since these imaged ocular structures are composed of collagen fibers, the analysis of their arrangement is investigated with the structure tensor. Details on this algorithm can be found in [45]. In brief, this is a mathematical tool used to explore the organization of fiber-like structures. It provides quantitative parameters related to the spatially resolved arrangement, such as the map of preferential orientations (PO) of the fibers and the structural dispersion (or alternatively, the level of organization). This latter is employed to classify collagen distribution into quasi-aligned, partially organized and nonorganized. Figure 2 depicts an illustrative example of two SHG images (human cornea) with the corresponding maps and histograms of PO. In particular, SDQI values of these SHG images are respectively 18 (healthy cornea, Fig. 2(a)) and 4 (diseased cornea, Fig. 2(c)).

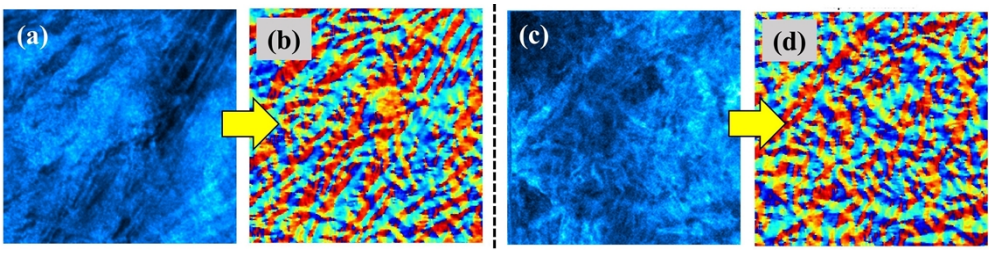

Fig. 2. SHG images of a healthy (a) and pathological (c) human cornea (image size: 180×180 µm^2). (b, d) Associated maps of PO.

Biomedical Optics EXPRESS

2.2. Deconvolution procedure

In MP, as in other retinal imaging and microscopy modalities, the imaging process is fundamentally three-dimensional and can be modeled (at least locally) as a 3D convolution of the 3D observed object with a 3D PSF, of which only a slice, i.e., a 2D image, is usually recorded. This constitutes a major difficulty, as estimating a 3D object from a 2D image is obviously very under-determined. To address this, we follow the approach of [39] assuming that, at least within the depth of field, the 3D object o_{3D} can be approximated as separable, i.e., is the product of a 2D object with a function $\alpha(z)$: $o_{3D}(x,y,z) = o_{2D}(x,y)\cdot\alpha(z)$, where $\alpha(z)$ can be interpreted as the normalized flux arriving from the plane at depth z. Within this approximation, the 3D deconvolution problem can be recast as a 2D blind deconvolution similar to the one encountered e.g. in Astronomy, in which the recorded 2D image is the 2D convolution of the 2D object $o_{2D}(x,y)$ with an unknown PSF. Additionally the latter, in the problem at hand, is the linear combination of the PSFs for all considered planes [39]. Considering a finite number of planes N_{planes} and discretizing the 2D object o_{2D} into a discrete sought object $\boldsymbol{o}$ yields the following discrete imaging model for the recorded 2D image $\boldsymbol{i}$:

$$i = o * h + noise, \tag{1}$$

with a discrete PSF given by:

$$h(k,l) = \sum_{j=1}^{N_{planes}} \alpha_j \cdot h_j(k,l). \tag{2}$$

The problem of estimating the object and the PSF remains under-determined, with an unknown object of the same size as the image plus the N_{planes} unknowns α_j that parameterize the PSF (typically $N_{planes} = 5$).

The conventional way of tackling this proem is to perform a blind (or "myopic") deconvolution, consisting of a joint estimation of both the sought object and the PSF, if possible with additional constraints such as PSF band-limitedness and positivity, object positivity and support, etc. (see [38] for a review). This has been shown to be reasonably effective in practice when these constraints are applicable, e.g. in Astronomy [46]. In biomedical imaging, where the object extends beyond the field of view and the image has a limited contrast, the object support constraint is inapplicable and the positivity is ineffective. In this case the joint blind deconvolution has been shown to be degenerate [39,47], in the sense that the estimation leads to a wrong couple (object, PSF) even if the noise level is arbitrarily small.

The problem lies in the fact that there are too many unknowns for too little data, i.e., the statistical contrast of our estimation, defined as the ratio of the number of data over the number of unknowns, remains lower than 1. The idea for a solution is to try and estimate "only" the PSF, on average for all possible objects within a given class. This idea is embodied in the so-called *marginal blind deconvolution* [39], where the likelihood of the data is marginalized over the unknown object (of a given Power Spectral Density (PSD)), and maximized as a function of the sole PSF, i.e., as a function of the N_{planes} coefficients α_j.

Finally, because the PSDs of the object and that of the noise are actually unknown, we must also estimate them. To this purpose, we use a sparse parameterization for the object's PSD with only three parameters [48], so that we only have a total of $N_{planes} + 4$ unknowns (N_{planes} for the PSF, 3 for the object's PSD and 1 for the noise PSD). This way, the statistical contrast of our estimation remains much greater than unity and the appealing theoretical properties of maximum likelihood estimation such as consistency are retained in practice, as verified by simulations [39].

Figure 3 shows a sketch of the overall procedure, which consists in firstly estimating the PSF and the PSDs by maximizing the marginalized likelihood, and secondly restoring the object by a conventional deconvolution with the estimated PSF. Here we use a Maximum A Posteriori deconvolution with Gaussian prior and white Gaussian noise assumptions (Wiener filter), taking as inputs the estimated object PSD and noise PSD, which makes the whole procedure entirely

Biomedical Optics EXPRESS

unsupervised. Note that this method has also been recently transposed successfully to Astronomy [49]. The deconvolution algorithm was written in IDL (Interactive Data Language).

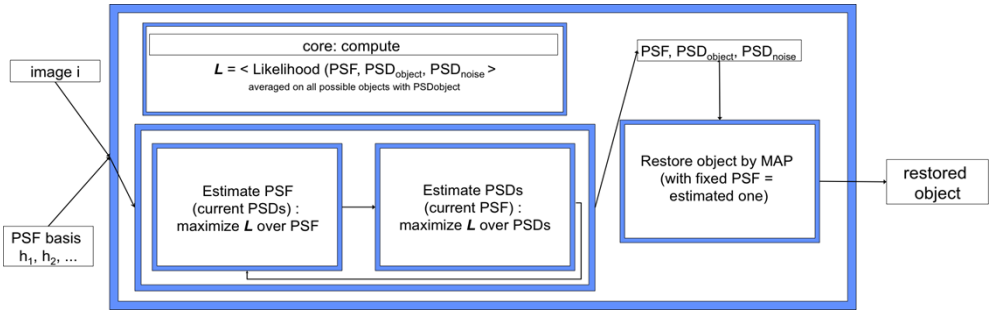

Fig. 3. Sketch of the marginal blind deconvolution procedure used in this work.

3. Results

3.1. Image deconvolution in ex-vivo tissues: a preliminary test

As a proof of concept, the technique was firstly tested with *ex-vivo* ocular tissues (i.e., static samples). SHG images of a human cornea (stroma) before and after deconvolution are depicted in Fig. 4(a) and 4(b). A simple visualization reveals the differences in the quality of the deconvolved image when compared to the original one. The histograms corresponding to the images are also shown (Fig. 4(c) and 4(d)). It can be observed how the histogram broadens in the restored image, what means an increase in the contrast. Moreover, while the total intensity keeps constant ($2.97{\cdot}10^4$ vs. $2.94{\cdot}10^4$ a.u.), the image quality after deconvolution provides a higher quality as measured through the acutance and the SDQI metric. In particular, for this example, acutance and SDQI increased from 2.20 to 22.45 (~10x) and from 6.06 to 23.45 (~4x) respectively.

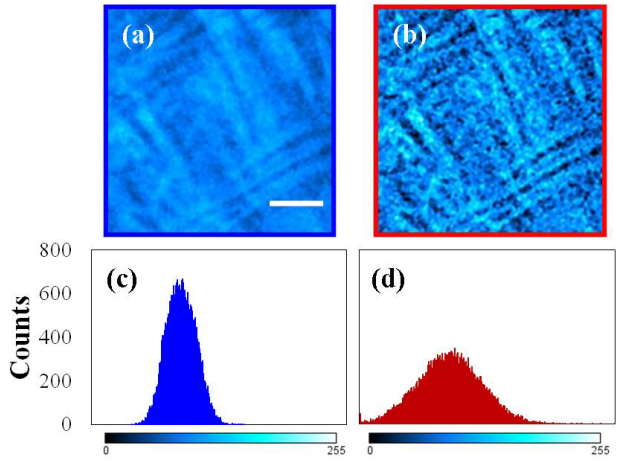

Fig. 4. Original (a) and deconvolved (b) SHG images of an *ex vivo* human cornea. The corresponding intensity histograms (c, d) are also shown. Scale bar: 50 µm.

At this point, it is known that the "true" PSF able to improve the SHG image cannot be measured. Then, the most appropriate demonstration of superiority of the present technique is to compare the SHG images deconvolved with that correct PSF and the result obtained using a

Biomedical Optics EXPRESS

"wrong" PSF. In this sense Fig. 5 figure presents the image restored using our marginal blind deconvolution method (Fig. 5(b)) and a classical deconvolution using a perfect PSF (Airy disc pattern, Fig. 5(c)). Unsurprisingly, the deconvolution using the wrong PSF provides an image with lower quality than that obtained when using the actual protocol.

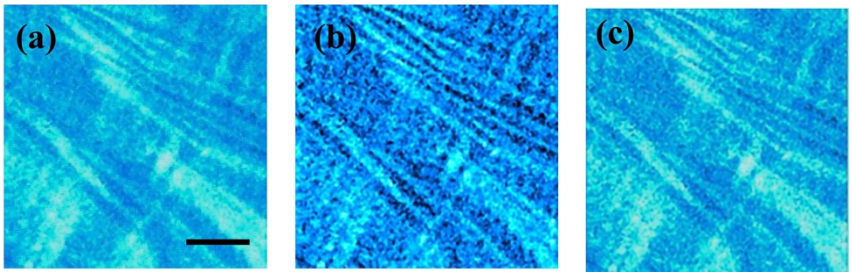

Fig. 5. Original SHG image of an *ex vivo* human cornea (a); image restored with our marginal blind deconvolution (b) and image restored using a perfect PSF, i.e. an Airy pattern, for lack of the knowledge of the true PSF (c). Bar length: 50 µm.

3.2. Deconvolution procedure in living human ocular tissues

Once the algorithm was successfully tested in static samples, it has been applied to *in vivo* SHG images. This is more interesting since apart from aberrations, images might also be affected by non-controlled micro-movements that further limit the performance of the acquisition device.

Figure 6 depicts two examples of living SHG images, one of the cornea (Fig. 6(a)) and the other for the sclera (Fig. 6(b)). The corresponding deconvolved images using the algorithm described herein are also shown (Fig. 6(c) and 6(d)). Both restored images display resolution improvement compared to the original ones. Collagen structures in the original images, although visible, they are less defined than in *ex vivo* images (see for instance Fig. 4(a) and 5(a)). However, after deconvolution fibers of different sizes and orientations are better observed as a result of the image quality improvement. Moreover, in the SHG images of the corneal stroma the crosshatched arrangement of the collagen bundles is also evident. The deconvolution operation does not modify the total intensity of the images (i.e. the energy is maintained).

Figure 7 depicts another example of after-deconvolution improvement as seen with the corresponding image intensity histograms. The imaged area corresponds to the sclero-corneal limbus. As claimed before, while the total intensity keeps constant, the histogram of the restored image is broader, what is associated with an increase in the contrast, then a better observation of structural features.

The increase in image quality occurred for all the SHG images evaluated along the experiment. This is plotted in Fig. 8 which presents the SDQI ratio (deconvolved vs. original) for all 10 *in vivo* images used herein. This ratio is above 1 for all SHG images (see horizontal red dotted line in the plot). Higher ratio values in this Fig. 8 correspond to a higher image improvement when comparing each restored/original image pair. Differences in values are reasonable since SHG images correspond to different areas of the cornea and the sclera. SDQI values are particular for each image (both original and restored) as distinct biological features (size, shape, orientation,. . .) are visualized. Then, the ratio between each pair of images is expected to vary.

For the sake of completeness, the performance of the algorithm was also evaluated at a local scale. Figure 9 shows another example where the change in local contrast has been evaluated along an intensity profile. Comparing SHG images, a noticeable increase in both contrast and resolution is readily observable. This leads to a better visualization of biological details. In

Biomedical Optics EXPRESS

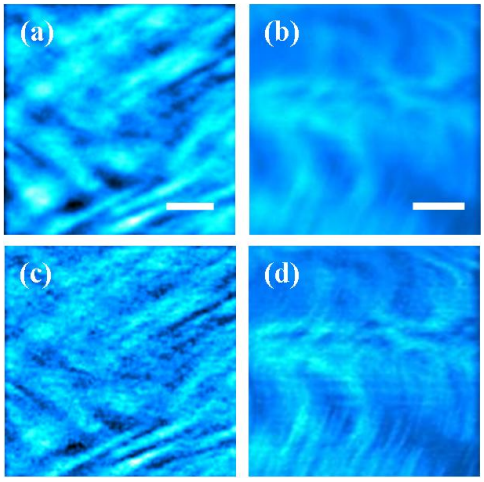

Fig. 6. Original (a, b) and deconvolved (c, d) SHG images of the living human cornea (a, c) and sclera (b, d). Scale bar: 50 µm.

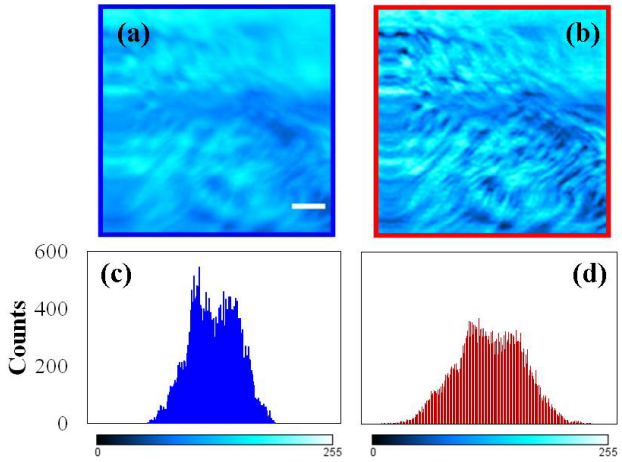

Fig. 7. SHG images of the *in vivo* sclero-corneal limbus: original (a) y deconvolved (b). Plots at the bottom are the correspond histograms (blue, original; red, deconvolved. Bar length: 50 µm.

Biomedical Optics EXPRESS

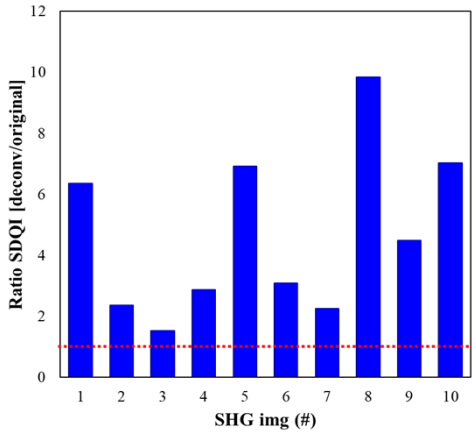

Fig. 8. Improvement in SDQI (deconvolved vs. original ratio) of all SHG images from the living human eye used in this work.

particular, the local contrast values increase from 0.16 and 0.44 respectively (that is, an increase of ~3x after deconvolution).

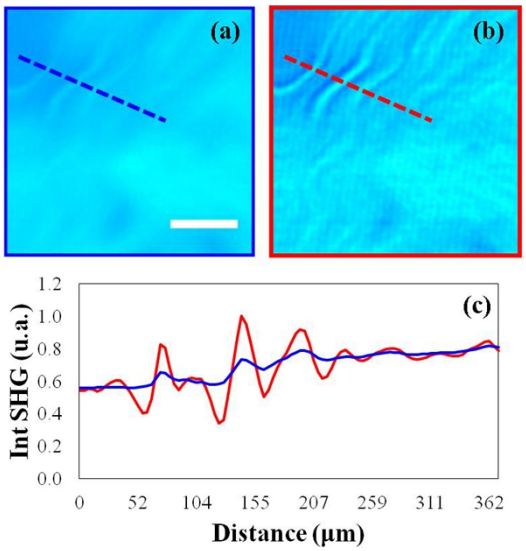

Fig. 9. SHG images before (a) and after (b) deconvolution. The intensity profiles of (c) are those corresponding to the lines indicated in the images. The imaged area corresponds to a temporal location of the sclera. Scale bar: 50 µm.

Once it has been shown how deconvolution is able to increase the image quality of SHG images of living human ocular tissues, it is interesting to explore if these enhanced images provide extra information on collagen arrangement. For this goal, the structure tensor has been used (see Section 2.1).

For representative SHG images of the living cornea and the sclera, Fig. 10 compares the maps of fiber preferential orientation computed from images before and after deconvolution. Whereas in the maps for the original images the detected fibers are thick and some of them missing, for the restored images narrower fibers are better resolved (see, for instance, reddish features

Biomedical Optics EXPRESS

within the maps). This is directly associated with the increase in resolution reached through the deconvolution method here proposed. It is worth noticing that this enhanced detection of individual fibers and their orientation might have relevant application in the detection and analysis of certain pathologies related to collagen disorders.

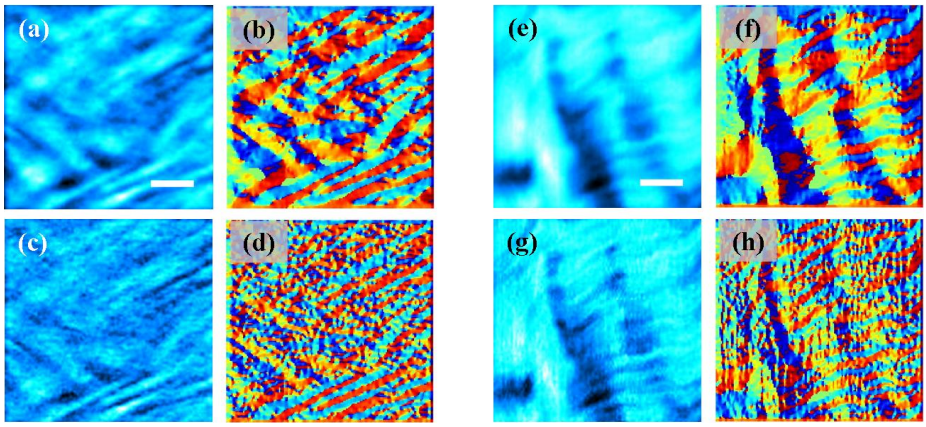

Fig. 10. SHG images before (a, e) and after (c, g) deconvolution. (b, d, f, h) Maps of preferential orientation. Imaged areas correspond to the cornea (a, c) and the sclera (e, g). Bar length: 50 µm.

4. Discussion and conclusions

For the last two decades, there has been considerable interest in the analysis of *ex vivo* collagen-based ocular tissues using SHG imaging microscopy (both healthy and pathological) [5–14]. Although SHG image acquisition of the human eye in living conditions is challenging, in our group we have been able to successfully report *in vivo* images of different structures under safety conditions using a custom compact and clinically-adapted microscope [20]. Despite the usefulness of SHG ocular images, the sample's aberrations represent a limitation. Moreover, in living conditions, movements and uncontrolled dynamics represent additional handicaps.

MP-AO procedures have been shown to improve MP microscopy images [24–26]. Although they were originally restricted to static samples, it use has been extended to living specimens [27–29]. On the other hand, the implementation of deconvolution techniques into different microscopes has been reported an alternative approach with interesting results [31–37].

Deconvolution is a powerful and low-cost high-resolution class of methods designed to compensate for image degradation. In microscopy (including retinal imaging), although the imaging process is fundamentally three-dimensional, with reasonable assumptions the deconvolution problem can be cast as a 2D blind deconvolution problem [39].

In order to enhance the quality of SHG microscopy images of the living human eye and to cope with the under-determined nature of the corresponding deconvolution problem, in this paper we have used the *marginal blind* approach of [39]: the unknown object is marginalized out of the problem, and only the PSF, the noise PSD and the object PSD are estimated. Then the image is deconvolved in a fully unsupervised way with the estimated PSF and PSDs.

Two features of the blind deconvolution procedure used here are quite unique, we dare say, in SHG microscopy context: firstly, as described in Section 2.2 and contrary to common methods, our deconvolution method takes into account the 3D nature of the imaging process. Secondly, unlike the commonly used joint estimation of the PSF and the object of interest, which has been shown to be a mathematically degenerate problem, our deconvolution method has the appealing statistical properties of Maximum Likelihood.

Biomedical Optics EXPRESS

The quality of the restored images was compared to that of the original ones in terms of objective metrics and feature visualization. The method was firstly validated on an *ex vivo* cornea sample and the advantages of its use was ready observable. The method proved to be also well suited for *in vivo* human ocular SHG imaging and the unsupervised estimation of enhanced images has also been shown. The benefit of using this method was demonstrated for SHG images of different living collagen-based ocular tissues and locations.

As it can be seen in the examples here reported, the quality of the images was always enhanced and collagen fibers were better visualized. All restored SHG images showed improved contrast and resolution. Although the quantitative boost depended on the metric and the imaged area, the use of different image quality metrics led to similar outcomes. In particular, the increase in SDQI (deconvolution vs. original ratio) ranged between 1.75 and 10 times.

However, the advantages of this deconvolution approach is not only limited to an increase in image quality. The analysis of the collagen arrangement obtained from restored SHG images indicates that the quantification of the structural organization might also benefit from enhanced images, since a more appropriate calculation of the collagen organization can be obtained. This is critical in clinical applications where an accurate calculation of the parameters of collagen spatial distribution serves as an objective tool for disease diagnosis [10]. If certain parameters providing information on collagen distribution are not correctly computed (mainly because of a non-appropriate quality of the image under study), the corresponding detection of pathologies might be over/underestimated, what would lead to erroneous pharmacological treatments or even unnecessary surgery.

Deconvolution and AO are useful techniques to improve MP microscopy images. However, SHG signal was also early recognized to depend on incident polarization [50]. Although this topic is out of the scope of this work, it is worth to notice that different homogeneous polarization states (mainly circular and linear) might provide different visualizations of biological details within an image [42,44,51]. Moreover, radial polarization provides even better SHG images than circular one [43]. The combination of polarization and AO into SHG microscopy has showed that the former adds extra benefits to the latter in terms of image quality enhancement [52]. Then, future implementations of a control polarization device into our compact clinically-oriented instrument, and a posterior deconvolution of those polarization-optimized *in vivo* SHG images might further enhance the outcome.

In conclusion, we have presented the application of a blind deconvolution technique tailored for microscopy to high-resolution SHG imaging of living human ocular tissues. The effectiveness of the approach was demonstrated, with a measurable improvement, which leads to better images with enhanced contrast and resolution, while keeping the total intensity constant. Independently of the imaged area and the dynamics nature of the eye, differences were ready visible when directly comparing pairs of SHG images (original and restored). Apart from increasing the image quality of SHG images, deconvolved images represent an additional benefit when applied to the study of collagen organization. Since more delineated structures appear and a better visualization of sharp features is obtained, the herein used method represents a powerful approach to obtain additional and accurate information from collagen-based tissues. This represents a further step towards early and accurate detection of pathologies related to non-controlled changes in collagen distribution at the fiber scale, not only in the eye, but also in other biomedical fields including pathological anatomy and cancer research among others.

Funding. Agencia Estatal de Investigación (PID2019-105684RB-I00/AEI/10.13039/501100011033, PID2020-113919RB-I00/AEI/10.13039/501100011033).

Disclosures. The authors declare no conflicts of interest and have no proprietary interest in any of the materials mentioned in this article.

Data availability. Data underlying the results presented in this paper are not publicly available at this time but may be obtained from the authors upon reasonable request.

Biomedical Optics EXPRESS

References

1. S. Fine and W. P. Hansen, "Optical second harmonic generation in biological systems," Appl. Opt. **10**(10), 2350–2353 (1971).
2. P. J. Campagnola, H. A. Clark, W. A. Mohler, A. Lewis, and L. M. Loew, "Second-harmonic imaging microscopy of living cells," J. Biomed. Opt. **6**(3), 277–286 (2001).
3. J. M. Bueno, F. J. Ávila, and P. Artal, "Second harmonic generation microscopy: a tool for quantitative analysis of tissues," in *Microscopy and Analysis*, S. G. Stanciu, ed. (IntechOpen, 2016).
4. B. F. Hochheimer, "Second harmonic light generation in the rabbit cornea," Appl. Opt. **21**(8), 1516–1518 (1982).
5. A. T. Yeh, N. Nassif, A. Zoumi, and B. J. Tromberg, "Selective corneal imaging using combined second-harmonic generation and two-photon excited fluorescence," Opt. Lett. **27**(23), 2082–2084 (2002).
6. F. Aptel, N. Olivier, A. Deniset-Besseau, J.-M. Legeais, K. Plamann, M.-C. Schanne-Klein, and E. Beaurepaire, "Multimodal nonlinear imaging of the human cornea," Invest. Ophthalmol. Vis. Sci. **51**(5), 2459–2465 (2010).
7. J. M. Bueno, E. J. Gualda, and P. Artal, "Analysis of corneal stroma organization with wavefront optimized nonlinear microscopy," Cornea **30**(6), 692–701 (2011).
8. M. Winkler, D. Chai, S. Kriling, C. J. Nien, D. J. Brown, B. Jester, T. Juhasz, and J. V. Jester, "Nonlinear optical macroscopic assessment of 3-D corneal collagen organization and axial biomechanics," Invest. Ophthalmol. Vis. Sci. **52**(12), 8818–8827 (2011).
9. A. Batista, H. G. Breunig, A. König, A. Schindele, T. Hager, B. Seitz, and K. König, "High-resolution, label-free two-photon imaging of diseased human corneas," J. Biomed. Opt. **23**(03), 1 (2018).
10. F. J. Ávila, P. Artal, and J. M. Bueno, "Quantitative discrimination of healthy and diseased corneas with second harmonic generation microscopy," Trans. Vis. Sci. Tech. **8**(3), 51 (2019).
11. M. Han, G. Giese, and J. Bille, "Second harmonic generation imaging of collagen fibrils in cornea and sclera," Opt. Express **13**(15), 5791–5797 (2005).
12. W. Lo, H.-Y. Tan, M.-G. Lin, C.-M. Hsueh, W.-L. Chen, S.-J. Lin, S.-H. Jee, and C.-Y. Dong, "Forward and backward second harmonic generation imaging of corneal and scleral collagen," Proc. SPIE **6860**, 68600F (2008).
13. H. Sun, R. M. Kurtz, and T. Juhasz, "Evaluation of human sclera after femtosecond laser ablation using two photon and confocal microscopy," J. Biomed. Opt. **17**(8), 081411 (2012).
14. M. Yamanari, S. Nagase, S. Fukuda, K. Ishii, R. Tanaka, T. Yasui, T. Oshika, M. Miura, and Y. Yasuno, "Scleral birefringence as measured by polarization-sensitive optical coherence tomography and ocular biometric parameters of human eyes *in vivo*," Biomed. Opt. Express **5**(5), 1391–1402 (2014).
15. M. Hao, K. Flynn, C. Nien-Shy, B. E. Jester, M. Winkler, D. J. Brown, O. La Schiazza, J. Bille, and J. V. Jester, "*In vivo* non-linear optical (NLO) imaging in live rabbit eyes using the Heidelberg two-photon laser ophthalmoscope," Exp. Eye Res. **91**(2), 308–314 (2010).
16. G. Latour, I. Gusachenko, L. Kowalczuk, I. Lamarre, and M. C. Schanne-Klein, "*In vivo* structural imaging of the cornea by polarization-resolved second harmonic microscopy," Biomed. Opt. Express **3**(1), 1–15 (2012).
17. H. L. Zhang, L. Wang, S. Liu, Y. Xie, X. Deng, S. He, J. Zhang, S. Sun, X. Li, and Z. Li, "Two-photon imaging of the cornea visualized in the living mouse using vital dyes," Invest. Opthalmol. Vis. Sci. **54**(10), 6526–6535 (2013).
18. J. H. Lee, S. Lee, Y. S. Gho, I. S. Song, H. Tchah, M. J. Kim, and K. H. Kim, "Comparison of confocal microscopy and two-photon microscopy in mouse cornea *in vivo*," Exp. Eye Res. **132**, 101–108 (2015).
19. T. Ehmke, J. Leckelt, M. Reichard, H. Weiss, M. Hovakimyan, A. Heisterkamp, O. Stachs, and S. Baltrusch, "*In vivo* nonlinear imaging of corneal structures with special focus on BALB/c and streptozotocin-diabetic Thy1-YFP mice," Exp. Eye Res. **146**, 137–144 (2016).
20. F. J. Ávila, A. Gambín, P. Artal, and J. M. Bueno, "In vivo two-photon microscopy of the human eye," Sci. Rep. **9**(1), 10121 (2019).
21. D. Débarre, E.J. Botcherby, T. Watanabe, S. Srinivas, M.J. Booth, and T. Wilson, "Image-based adaptive optics for two-photon microscopy," Opt. Lett. **34**(16), 2495–2497 (2009).
22. J. M. Bueno, M. Skorsetz, R. Palacios, E. J. Gualda, and P. Artal, "Multiphoton imaging microscopy at deeper layers with adaptive optics control of spherical aberration," J. Biomed. Opt. **19**(1), 011007 (2013).
23. J. M. Bueno, R. Palacios, A. Pennos, and P. Artal, "Second-harmonic generation microscopy of photocurable polymer intrastromal implants in ex-vivo corneas," Biomed. Opt. Express **6**(6), 2211–2219 (2015).
24. M. J. Booth, "Adaptive optical microscopy: the ongoing quest for a perfect image," Light: Sci. Appl. **3**(4), e165 (2014).
25. N. Ji, "Adaptive optical fluorescence microscopy," Nat. Methods **14**(4), 374–380 (2017).
26. J. M. Bueno, "Adaptive optics in multiphoton microscopy," in *Advanced Optical Methods for Brain Imaging*, F.-J. Kao, G. Keiser, and A. Gogoi, eds., (Springer Nature, 2019).
27. A. Jesacher, A. Thayil, K. Grieve, D. Débarre, T. Watanabe, T. Wilson, S. Srinivas, and M. Booth, "Adaptive harmonic generation microscopy of mammalian embryos," Opt. Lett. **34**(20), 3154–3156 (2009).
28. N. Ji, T. R. Sato, and E. Betzig, "Characterization and adaptive optical correction of aberrations during in vivo imaging in the mouse cortex," Proc. Natl. Acad. Sci. **109**(1), 22–27 (2012).
29. K. Wang, D. E. Milkie, A. Saxena, P. Engerer, T. Misgeld, M. E. Bronner, J. Mumm, and E. Betzig, "Rapid adaptive optical recovery of optimal resolution over large volumes," Nat. Methods **11**(6), 625–628 (2014).
30. C. Rodríguez and N. Ji, "Adaptive optical microscopy for neurobiology," Curr. Opin. Neurobiol. **50**, 83–91 (2018).

Biomedical Optics EXPRESS

31. P. J. Verveer, M. J. Gemkow, and T. M. Jovin, "A comparison of image restoration approaches applied to three-dimensional confocal and wide-field fluorescence microscopy," J. Microsc. **193**(1), 50–61 (1999).
32. P. Sarder and A. Nehorai, "Deconvolution methods for 3-D fluorescence microscopy images," IEEE Signal Process. Mag. **23**(3), 32–45 (2006).
33. H. Yoo, I. Song, and D.-G. Gweon, "Measurement and restoration of the point spread function of fluorescence confocal microscopy," J. Microsc. **221**(Pt 3), 172–176 (2006).
34. N. Chakrova, B. Rieger, and S. Stallinga, "Deconvolution methods for structured illumination microscopy," J. Opt. Soc. Am. A **33**(7), B12–B20 (2016).
35. A. Doi, R. Oketani, Y. Nawa, and K. Fujita, "High-resolution imaging in two-photon excitation microscopy using in situ estimations of the point spread function," Biomed. Opt. Express **9**(1), 202–213 (2018).
36. Y. Lai-Tim, L. M. Mugnier, F. Orieux, R. Baena-Gallé, M. Paques, and S. Meimon, "Jointly super-resolved and optically sectioned Bayesian reconstruction method for structured illumination microscopy," Opt. Express **27**(23), 33251–33267 (2019).
37. Y. Lai-Tim, L. M. Mugnier, L. Krafft, A. Chen, C. Petit, P. Mecê, K. Grieve, M. Paques, and S. Meimon, "Super-resolution in vivo retinal imaging using structured illumination ophthalmoscopy," arXiv, 2007.16028 (2020).
38. L. Blanc-Féraud, L. Mugnier, and A. Jalobeanu, "Blind image deconvolution," in *Inverse Problems in Vision and 3D Tomography*, A. Mohammad-Djafari, ed., (John Wiley, 2010).
39. L. Blanco and L. M. Mugnier, "Marginal blind deconvolution of adaptive optics retinal images," Opt. Express **19**(23), 23227–23239 (2011).
40. Y. F. Choong, F. Rakebrandt, R. V. North, and J. E. Morgan, "Acutance, an objective measure of retinal nerve fibre image clarity," Br. J. Ophthamol. **87**(3), 322–326 (2003).
41. M. Rakhshanfar and M. A. Amer, "Sparsity-based no-reference image quality assessment for automatic denoising," J. Signal, Image and Video Processing **12**(4), 739–747 (2018).
42. S. G. Stanciu, F. J. Ávila, R. Hristu, and J. M. Bueno, "A study on image quality in polarization-resolved second harmonic generation microscopy," Sci. Rep. **7**(1), 15476 (2017).
43. R. M. Martínez-Ojeda, C. Hernández-García, and J. M. Bueno, "Enhancement of second harmonic microscopy images in collagen-based thick samples using radially polarized laser beams," Opt. Commun. **499**, 127273 (2021).
44. J. M. Bueno, R. M. Martínez-Ojeda, I. Yago, and F. J. Ávila, "Collagen organization, polarization sensitivity and image quality in human corneas using second harmonic generation microscopy," Photonics **9**(10), 672 (2022).
45. F. J. Ávila and J. M. Bueno, "Analysis and quantification of collagen organization with the structure tensor in second harmonic microscopy images of ocular tissues," Appl. Opt. **54**(33), 9848–9854 (2015).
46. L. M. Mugnier, T. Fusco, and J.-M. Conan, "MISTRAL: a myopic edge-preserving image restoration method, with application to astronomical adaptive-optics-corrected long-exposure images," J. Opt. Soc. Am. A **21**(10), 1841–1854 (2004).
47. A. Levin, Y. Weiss, F. Durand, and W. T. Freeman, "Understanding blind deconvolution algorithms," IEEE Trans. Pattern Anal. Mach. Intell. **33**(12), 2354–2367 (2011).
48. J.-M. Conan, L. M. Mugnier, T. Fusco, V. Michau, and G. Rousset, "Myopic deconvolution of adaptive optics images by use of object and point-spread function power spectra," Appl. Opt. **37**(21), 4614–4622 (1998).
49. R. J-L. Fétick, L. M. Mugnier, T. Fusco, and B. Neichel, "Blind deconvolution in astronomy with adaptive optics: the parametric marginal approach," Mon. Not. R. Astron. Soc. **496**(4), 4209–4220 (2020).
50. S. Roth and I. Freund, "Second harmonic generation in collagen," J. Chem. Phys. **70**(4), 1637–1643 (1979).
51. F. J. Avila, O. del Barco, and J. M. Bueno, "Polarization dependence of aligned collagen tissues imaged with second harmonic generation microscopy," J. Biomed. Opt. **20**(8), 086001 (2015).
52. J. M. Bueno, F. J. Ávila, R. M. Martínez-Ojeda, and P. Artal, "Adaptive-optics polarization-sensitive second harmonic generation microscopy," *2020 22nd International Conference on Transparent Optical Networks (ICTON)*, Bari, Italy, 1–4 (2020).

155.54.207.227 {ts '2023-04-24 03:17:21'}